OPTIMAL OPEN-LOOP RAM VELOCITY PROFILES FOR ISOTHERMAL FORGING: A VARIATIONAL APPROACH

By

Jordan M. Berg
W. Garth Frazier
Anil Chaudhary
and
Siva S. Banda

IMA Preprint Series # 1389
March 1996

INSTITUTE FOR MATHEMATICS AND ITS APPLICATIONS
UNIVERSITY OF MINNESOTA
514 Vincent Hall
206 Church Street S.E.
Minneapolis, Minnesota 55455

Optimal Open-Loop Ram Velocity Profiles for Isothermal Forging: A Variational Approach

Jordan M. Berg
USAF Wright Laboratory, WL/FIGC, Dayton, OH

W. Garth Frazier
Cedarville College, Cedarville, OH

Anil Chaudhary
USAF Wright Laboratory, WL/MLIM, Dayton, OH

Siva S.Banda
USAF Wright Laboratory, WL/FIGC, Dayton, OH

Abstract

A successful forging attains both a desired final shape, and a desired final internal microstructure. Therefore it is desirable to incorporate knowledge of microstructural transformation mechanisms into the design of the forging process parameters. This paper applies tools from the variational calculus to solve the problem of selecting an open-loop ram velocity profile for an isothermal forging. It is assumed that a desired effective strain rate, expressed as a function of effective strain and temperature, is available to specify optimal processing conditions for the material. A weighting function is selected that reflects the rate at which the internal microstructure is transforming. The material flow is modeled using a nonlinear finite-element code. Under certain reasonable assumptions, the algorithm is shown to yield a globally optimal solution. The method is demonstrated for the simulated forging of a TiAl compressor disk.

1 Introduction

Bulk forming processes such as forging are invaluable for producing metal parts with desirable mechanical properties. These mechanical properties correspond to a particular material microstructure. Thus a successful forging produces both a desired shape, and a desired microstructure. Figure 1 portrays an idealized forging. The design of these processes is still largely an art. The goal of this work is to integrate mathematical models of microstructural evolution with detailed numerical simulations of the deforming billet, in a systematic approach to ram velocity design. The current effort was motivated by ideas presented by Malas, *et al.* (1992; 1993), and represented for the purpose of this paper by Fig. 2. There are two independent stages. The given initial microstructure and desired final microstructures are the inputs to the first stage. The result is an optimal "material trajectory" in a three dimensional space of effective strain, effective strain rate, and temperature. This trajectory depends only on the material being forged, and is independent of the billet and die geometry. The second stage, with which this paper is solely concerned, is the generation of a ram velocity that will best enforce the optimal material trajectory. This paper will slightly extend the framework of Fig. 2, by incorporating microstructural evolution models into the calculations of stage 2.

The bulk forming variables that most profoundly influence the internal microstructure are the temperature, T, the effective strain rate, $\dot{\varepsilon}$, and the effective strain, ε. The effective strain rate is a non-negative scalar, related to the Euclidean norm of the strain rate tensor. The effective strain is the time integral of the effective strain rate, following a material point in the flowing metal. Of these, the temperature is usually the most critical. However, materials which must be formed at high temperatures and low strain rates are often forged in a temperature-regulated furnace. In such *isothermal forgings*, once the temperature has been selected, the effective strain rate is the most important factor remaining for developing proper microstructure. This paper is concerned only with isothermal forging. It is assumed that the temperature calculated in the first part of Fig. 2 is the constant forging temperature. Then the optimal material trajectory can be specified in the form $\dot{\varepsilon} = f(\varepsilon, T)$, where T is a constant parameter. Since the following development never uses the strain or strain rate tensors, ε and $\dot{\varepsilon}$ will often be referred to simply as the strain and strain rate.

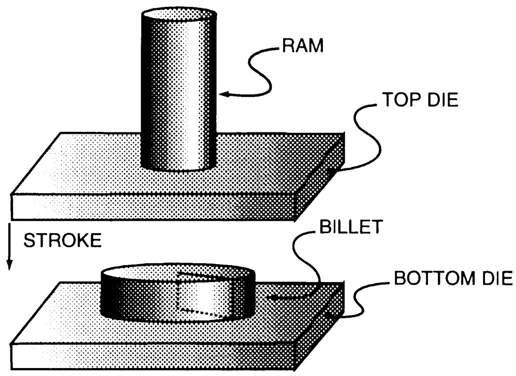

Fig. 1. Idealized forging schematic.

Good models are critical to the success of the optimal design procedure. Models of both the microstructural evolution and the workpiece flow field are required. The flow field is calculated using a standard nonlinear finite element code, treating the material as rigid-viscoplastic. This approximation is appropriate for the large strains expected in a forging. Furthermore, the method used may require many iterations through the FEM solver, and the rigid-viscoplastic representation is much faster than full elastoplastic models. Good automeshing is necessary to permit full automated calculation. Automeshing is standard in 2-D codes, but somewhat less so in 3-D codes. However, such packages are now becoming available, and the procedure presented below should then apply to 3-D parts without modification. The state of the art in microstructural modeling is far less advanced. The example presented here uses polynomial curve fits to compression test data.

Earlier efforts, which have led up to the current paper are reported in Berg, Adams, Malas, and Banda (1995) and Berg, Chaudhary, and Malas (1995). The first paper includes an introduction to the forging problem from a controls viewpoint. Other related works in the literature include an approach based on the LQR in Grandhi, *et al.* (1993), and Malas, Irwin, and Grandhi (1993), and a closed-loop, receding horizon controller described by Meyer (1993). The closed-loop approach of Meyer is not appropriate here, due to the lack of direct microstructure measurements. An indirect approach that does use feedback is described by Schwartz, *et al.* (1995). Many studies have been made of die and preform design to achieve a desired final shape. In the context of this paper, Maniatty and Chen (1995) is notable for its consideration of internal states such as microstructure.

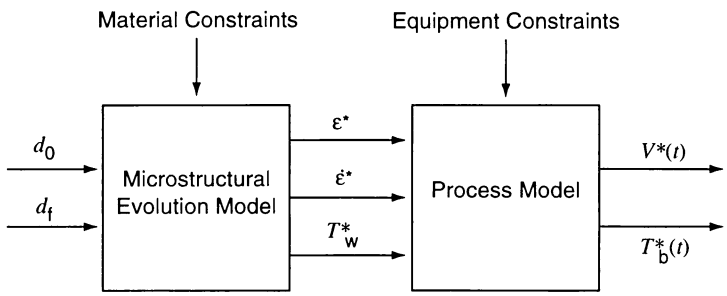

Fig. 2. Two step forging process design procedure, from Malas (1992).

Section 2 presents a variational formulation for selecting an unconstrained ram velocity profile. Section 3 shows how microstructural models can be introduced through weighting functions.Section 4 presents a numerical algorithm for solving the variational problem. Section 5 gives simulation results for a sample case: a 2-D axisymmetric compressor disk formed from a TiAl intermetallic.

2 The Variational Formulation

The object of this paper is to calculate a ram velocity profile that best tracks an optimal material trajectory. The optimal material trajectory is calculated based on material properties only, and is decoupled from the bulk forming problem. Malas, Irwin, and Grandhi (1993) present one approach to determining such a trajectory. In the current work, the optimal material trajectory is given in the following form:

$$\dot{\varepsilon} = f\left(\varepsilon\right) \tag{1}$$

Although the optimal material trajectory also has a temperature dependence, only isothermal forgings are considered here. Therefore T is simply a constant parameter, and it has been omitted for brevity.

The following variational problem is one way to track the optimal material trajectory:

$$\min_{v_{ram}(t)} \int_0^{t_f} \left\{ \int_\Omega W(\bullet)\left(f\left(\varepsilon_p\right) - \dot{\varepsilon}_p\right)^2 dV \right\} dt \tag{2}$$

subject to the constraint that the ram velocity be admissible.

The subscript p indicates that the strain rate and strain are at a particular point of material. The inner integral is a volume integral, taken over every point p in the workpiece, denoted by Ω The function W is a weighting. At this point, the form and functional dependence of W will not be specified. That is the subject of Section 3.

The velocity must be non-negative because reversing the ram will cause the die to separate from the billet. It is very useful, for purposes of analysis, to strengthen this requirement, and prohibit zero ram velocity. In practice, this will not be a significant restriction. The forging time be finite, and the required final stroke must be attained. The ram velocity must be bounded. Thus an admissible ram velocity is a function from $[0,t_f]$ to $(0,M]$.

The ram velocity itself does not appear directly in (2). The mapping between the ram velocity profile and the process variables ε, $\dot{\varepsilon}$, and T is given by a nonlinear partial differential equation with evolving boundary conditions (Hill, 1950; Oh, 1982). In general, very little can be said about this mapping. However the following observation for isothermal forgings proves to be surprisingly powerful:

Rate Invariance*: Fix the die and preform geometry. Then the evolving shape of the workpiece, and the effective strain distribution history, depend very strongly on the ram stroke, and weakly or not at all on the ram velocity profile.*

Simulations indicate that rate invariance is a very reasonable approximation for many isothermal forgings. The forging is assumed to be completely rate invariant, but this assumption will be verified in the example.

A rate-invariant forging problem may be simplified immensely by using stroke instead of time as the independent variable. The first application of this transformation will be to derive an extremely useful restatement of rate invariance. The second will be to rewrite the variational formulation (2) in an easy-to-solve form.

Let x denote the ram stroke, and $\dot{x}$ the corresponding ram velocity. The strictly positive $\dot{x}$ implies a strictly increasing x. Therefore, given any admissible stroke profile $x = X(t)$, mapping the interval $[0, t_f]$ to $[0, x_f]$, there is an inverse function, $\Theta:[0, x_f]\to[0, t_f]$, satisfying

$$x = X(\Theta(x)) \tag{3a}$$

Applying the chain rule gives,

$$\dot{X}(\Theta(x))\ \Theta'(x) = 1$$

or,

$$\Theta'(x) = \frac{1}{\dot{X}(\Theta(x))} \tag{3b}$$

Define $v(x) \overset{\text{def}}{=} \dot{X}(\Theta(x)))$. Now time may be eliminated from the problem completely, and replaced everywhere by stroke, as the independent variable.

By definition, ε is the time integral, following a particle, of the effective strain rate $\dot{\varepsilon}$.

$$\varepsilon_p(t) = \int_0^t \dot{\varepsilon}_p(\tau)\, d\tau \tag{4}$$

Apply the change of variables formula, using $t = \Theta(x)$.

$$\varepsilon_p(\Theta(x)) = \int_0^x \dot{\varepsilon}_p(\Theta(\zeta))\, \Theta'(\zeta)\, d\zeta \tag{5a}$$

or,

$$\tilde{\varepsilon}_p(x) = \int_0^x \dot{\tilde{\varepsilon}}_p(\zeta)\, \frac{1}{v(\zeta)}\, d\zeta \tag{5b}$$

Then rate invariance implies that $\tilde{\varepsilon}_p(x)$ is independent of the velocity profile $v(x)$. That implies that the strain rate, as a function of stroke, must have the form,

$$\dot{\tilde{\varepsilon}}_p(x) = h_p(x)\, v(x) \tag{6}$$

By definition $\dot{\varepsilon}$ is non-negative. Since the ram velocity is strictly posititve, $h_p(x)$ must be non-negative for all x. Rate invariance requires the *existence* of a function $h_p(x)$. Nowhere in the following is the function required to be *known*.

The cost function used in (2) can now be rewritten, applying the substitutions (5b) and (6).

$$J(x(t), \dot{x}(t)) = \int_0^{t_f} \left\{ \int_\Omega \tilde{W}_p\big(x(t)\big)\Big(\tilde{f}_p\big(x(t)\big) - h_p\big(x(t)\big)\,\dot{x}(t)\Big)^2 dV \right\} dt \tag{7}$$

where, anticipating the discussion of the next section, the weighting depends only on p and x. The problem of minimizing (7) is of the form,

$$\min_{x(t)} \int_0^{t_f} g(x(t), \dot{x}(t))\, dt \tag{8}$$

subject to the restrictions $x(0) = 0$, $x(t_f) = x_f$, $\dot{x} \in (0,\infty)$. Apply the change of variables $t = \Theta(x)$ to the integral in (8).

$$\int_0^{t_f} g(x(t), \dot{x}(t))\, dt = \int_0^{x_f} g(x(\Theta(x)), \dot{x}(\Theta(x)))\, \Theta'(x)\, dx$$
$$= \int_0^{x_f} g(x, v(x)) \frac{1}{v(x)}\, dx \tag{9}$$

Therefore the problem can be restated as,

$$\min_{v(x)} \int_0^{x_f} \frac{g(x, v(x))}{v(x)}\, dx \tag{10}$$

where x is now the independent variable, and,

$$g(x, v) = \int_\Omega \tilde{W}_p(x)\left(\tilde{f}_p(x) - h_p(x)\, v\right)^2 dV \tag{11}$$

Expand (11), and bring v, which has no p dependence, outside the integral.

$$g(x, v) = A(x)\, v^2 + B(x)\, v + C(x) \tag{12a}$$

where

$$A(x) \underline{\underline{\mathrm{def}}} \int_\Omega \tilde{W}_p(x)\, h_p^2(x) dV \tag{12b}$$

$$B(x) \underline{\underline{\mathrm{def}}} -2\int_\Omega \tilde{W}_p(x)\, \tilde{f}_p(x)\, h_p(x) dV \tag{12c}$$

$$C(x) \underline{\underline{\mathrm{def}}} \int_\Omega \tilde{W}_p(x)\, \tilde{f}_p{}^2(x)\, dV \tag{12d}$$

So the functional to be minimized is,

$$J(v(x)) = \int_0^{x_f} \left(A(x)\, v(x) + B(x) + \frac{C(x)}{v(x)} \right) dx \tag{13}$$

If the integrand is a continuous function of x, then a necessary condition for optimality is that the first variation of J be zero. The first variation is calculated by replacing $v(x)$ by $v(x)$

$+ \tau\eta(x)$, and differentiating with respect to τ (Axelsson and Barker, 1984). Then setting $\tau = 0$ gives,

$$J_\tau(v(x);\eta(x)) = \int_0^{x_f} \left(A(x) - \frac{C(x)}{v^2(x)} \right) \eta(x)\, dx \tag{14}$$

(14) is zero for arbitrary $\eta(x)$ if and only if,

$$v^2(x) = \frac{C(x)}{A(x)} \tag{15a}$$

Assuming for the moment that the RHS of (15) is defined and non-negative for all x in $[0,x_f]$, the function

$$v(x) = \sqrt{C(x)/A(x)} \tag{15b}$$

is a candidate for optimality. In fact, as is now shown, it is a unique global minimizer of (13).

(**GO**) *Unique Global Optimality of* $v(x)$. Assume that $A(x)$, $B(x)$ and $C(x)$ are defined, that $A(x) \neq 0$, and that $A(x)/C(x) \geq 0$, for all x in $[0,x_f]$. Let $v(x) = \sqrt{C(x)/A(x)}$ be the resulting ram stroke profile. Then $v(x)$ is a unique global minimizer of (13).

Proof: Substitute $v(x) = \sqrt{C(x)/A(x)}$ into (13).

$$J(v(x)) = \int_0^{x_f} \left(A(x) \frac{\sqrt{C(x)}}{\sqrt{A(x)}} + B(x) + C(x) \frac{\sqrt{A(x)}}{\sqrt{C(x)}} \right) dx$$

$$= \int_0^{x_f} \left(\sqrt{A(x)\, C(x)} + B(x) + \sqrt{A(x)\, C(x)} \right) dx$$

$$= \int_0^{x_f} \left(B(x) + 2\sqrt{A(x)\, C(x)} \right) dx$$

Next let $w(x)$ be any admissible ram velocity profile,

$$J(w(x)) = \int_0^{x_f} \left(A(x)\, w(x) + B(x) + \frac{C(x)}{w(x)} \right) dx$$

$$= \int_0^{x_f} \left(B(x) + 2\sqrt{A(x)\, C(x)} \right) dx + \int_0^{x_f} \left(\sqrt{A(x)\, w(x)} - \sqrt{\frac{C(x)}{w(x)}} \right)^2 dx$$

$$= J(v(x)) + \int_0^{x_f} \left(\sqrt{A(x)\, w(x)} - \sqrt{\frac{C(x)}{w(x)}} \right)^2 dx$$

So for any admissible $w(x)$, $J(w(x)) - J(v(x)) \geq 0$. Furthermore, equality holds if and only if $w(x) = \sqrt{C(x)/A(x)} = v(x)$. Therefore $v(x)$ is the unique global minimizer. ■

The proof is direct, so no special consideration of continuity or differentiability is required. Of course, it remains to show that the assumptions on $A(x)$, $B(x)$ and $C(x)$ are reasonable, and to ensure that the resulting velocity profile is admissible.

For realistic forgings and reasonable f and W, the integrals (12b-d) will exist. It is sufficient that these functions be bounded, piecewise-continuous, functions of their arguments on the full stroke interval. $h_p(x)$ need only be bounded, and a piecewise-continuous function of p. If the weighting function $\tilde{W}_p(x)$ is also non-negative, a very reasonable restriction, then $A(x)$, $B(x)$ and $C(x)$ are also non-negative. Finally, consider $A(x)$. Since $h_p(x)$ is at p only when that point of the billet is rigid, it is reasonable to assume that $h_p(x)$ is never zero for all p at any x in $[0, x_f]$. So by setting a minimum value for the weighting, $W_{\min} > 0$, the condition $A(x) \neq 0$ will be satisfied. Therefore the conditions of (**GO**) are easily and naturally satisfied, and (15b) is the globally optimal solution.

For the resulting $v(x)$ to be admissible, it must be bounded, and it must correspond to a ram stroke profile that reaches full stroke in finite time. These are ensured by requiring that, in addition to being bounded above, $f(\varepsilon)$ and $h_p(x)$ are also bounded below by strictly positive quantities. Recall that such a lower bound has already been assumed for $\tilde{W}_p(x)$.

To determine the transformation $t = \Theta(x)$, and so the forging time, write,

$$t = \int_0^x \frac{d\zeta}{v(\zeta)} = \Theta(x) \tag{16}$$

which defines implicitly the extremal ram profile $x = X(t)$. Since $v(x)$ is bounded below, say by δ_v, $t_f = \Theta(x_f)$ is bounded above by x_f/δ_v.

The development above is largely due to replacing time by stroke as the independent variable. This naturally leads to the question, what is so special about (13)? Why not replace the time integral in (8) with a stroke integral? The result is the new cost function,

$$\bar{J}(v(x)) = \int_0^{x_f} \left(A(x)\, v^2(x) + B(x)\, v(x) + C(x) \right) dx \tag{17}$$

This is a quadratic functional, and it is easy to show that a unique, globally optimal, solution is given by $v(x) = -B(x)/2A(x)$ (Axelsson and Barker, 1984). Under the same assumptions as made above, this solution will be admissible.

3 The Weighting Function

This section presents a weighting function that incorporates microstructural evolution behavior. The weighting function will be modified, if necessary, to satisfy the requirements of the previous section.

Why is a weighting function necessary? In the most simple of forgings—frictionless, axisymmetric, upsetting—the effective strain rate (and, if the initial billet is homogeneous, the effective strain) is uniform throughout the workpiece. Then if the optimal material trajectory is the same for all points, the desired profile can be exactly achieved, and no weighting is required. For a forging of any complexity, however, the strain rates may vary by several orders of magnitude across the billet at any given stroke. This means that not all points in the billet can possibly track the desired material trajectory. Then the designer must decide the relative importance of different material points.

How might the weighting function be chosen? A good weighting strategy should exploit the dynamics of the microstructural evolution. For example, consider a microstructural transformation mechanism that follows an Avrami-type behavior. That is, no transformation occurs until a critical strain level is reached. The graph of fraction of material transformed vs. strain then traces a sigmoidal curve, reaching 0.5 in a characteristic strain increment $\varepsilon_{1/2}$, and rising to over 0.99 in 3 such increments, thereafter asymptotically approaching full transformation. Such behavior has been observed in dynamic transformation mechanisms in plain carbon steel (Senuma and Yada, 1986) and TiAl intermetallics (Malas and Seetheraman, 1992). If the optimal material trajectory represents an ideal transformation path, what meaning can it have below the critical strain, where no material is transforming? Likewise, what significance can it have more than $3\varepsilon_{1/2}$ above the critical strain, when the transformation is nearly complete? The weighting described below reflects these considerations.

The development here is based upon a model of the dominant microstructural transformation mechanism with the following form:

$$d = d(\varepsilon, \dot{\varepsilon}, T) \tag{18a}$$

$$S = S(\varepsilon, T) \tag{18b}$$

Here d describes the relevant characteristic of the transformed microstructure—average grain size, for example—and S is the fraction of material that has transformed. The key feature for deriving a weighting function is that S be independent of time and $\dot{\varepsilon}$. Now, define the weighting at stroke x to be dS/dx. Omit the temperature dependence, because the forging is isothermal.

$$
\begin{aligned}
W &= \frac{\mathrm{d}\,S(\varepsilon)}{\mathrm{d}x} \\
&= \frac{\partial S}{\partial \varepsilon}\frac{\partial \varepsilon}{\partial x} = \frac{\partial S}{\partial \varepsilon}\frac{\dot{\varepsilon}}{\dot{x}} \\
&= \frac{\partial S}{\partial \varepsilon}\frac{\dot{\varepsilon}}{v} \overset{\text{def}}{=} W(\varepsilon, \dot{\varepsilon}, v) && \text{(19a)} \\
&= \frac{\partial S}{\partial \varepsilon}(Hp(x))\, h_p(x) \overset{\text{def}}{=} \tilde{W}_p(x) && \text{(19b)}
\end{aligned}
$$

Physically, the weighting (19) represents the fraction of material at point p that will be transforming over an infinitesimal stroke increment, dx. Therefore, at any given stroke, the strain rate in portions of material that are undergoing significant amounts of microstructural transformation is kept close to the ideal value, while the strain rate in other parts of the workpiece is allowed to deviate from the ideal. The transformation is assumed to progress in only one direction. That is, $\partial S/\partial\varepsilon$, and therefore $\tilde{W}_p(x)$, are non-negative. It may be necessary to apply lower and upper limits to (19) in order to comply with the requirements of the previous section.

4 Numerical Solution of the Variational Problem

The function $v(x) = \sqrt{C(x)/A(x)}$ globally minimizes (13). Unfortunately, the function $h_p(x)$ is not known, so $A(x)$ and $C(x)$ cannot be calculated. The only available information relating stroke and ram velocity to strain and strain rate is given by the nonlinear FEM code used to solve the nonlinear PDE. So rewrite (15a) as $C(x) - A(x)\, v^2(x) = 0$, and bring the terms under one integral,

$$\int_\Omega \tilde{W}_p(x)\left(\tilde{f}_p{}^2(x) - h_p^2(x)\, v^2\right) dV = 0 \tag{20}$$

Now replace the functions of x by the original functions of ε and $\dot{\varepsilon}$.

$$\int_\Omega W(\varepsilon_p, \dot{\varepsilon}_p, v)\left(f^{\,2}(\varepsilon_p) - \dot{\varepsilon}_p^2\right) dV = 0 \tag{21a}$$

Since the FEM discretizes the workpiece, (21a) is replaced by the sum, over all elements,

$$\sum_i \left\{ W\left(\varepsilon_i, \dot{\varepsilon}_i, v\right)\left(f^{\,2}\left(\varepsilon_i\right) - \dot{\varepsilon}_i^2\right) \right\} V_i = 0 \tag{21b}$$

where V_i is the volume of the i^{th} element. The LHS of (21b) can be evaluated by running the FEM process simulation at a particular stroke and ram velocity. At any given stroke, the problem of finding the optimal ram velocity now reduces to searching over all positive v for a root of (21b). By the results of the previous section, such a root must exist, and there is only one.

The corresponding functions for the alternative performance objective (17) are,

$$\int_\Omega W(\varepsilon_p, \dot{\varepsilon}_p, v)\left(\frac{\dot{\varepsilon}_p}{v}\right)\left(f\,(\varepsilon_p) - \dot{\varepsilon}_p\right) dV = 0 \tag{22a}$$

$$\sum_i \left\{ W\left(\varepsilon_i, \dot{\varepsilon}_i, v\right) \frac{\dot{\varepsilon}_i}{v} \left(f\left(\varepsilon_i\right) - \dot{\varepsilon}_i\right) \right\} V_i = 0 \tag{22b}$$

The special case of constant $f(\varepsilon)$ offers some insight into the meaning of (21) and (22). In that case, (21a) becomes,

$$\frac{\int_\Omega \dot{\varepsilon}_p^2\, W dV}{\int_\Omega W dV} = \frac{\int_\Omega \dot{\varepsilon}_p^2\, dV_W}{V_W} = \overline{\dot{\varepsilon}^2} = f^{\,2} \tag{23}$$

In other words, the root-mean-square strain rate should track the desired strain rate. Here the mean is understood to be with respect to the weighted volume. Likewise, (22a) becomes,

$$\frac{\int_{\Omega} \dot{\varepsilon}_p^2 \, W dV}{\int_{\Omega} \dot{\varepsilon}_p \, W dV} = \frac{V_W \int_{\Omega} \dot{\varepsilon}_p^2 \, dV_W}{V_W \int_{\Omega} \dot{\varepsilon}_p \, dV_W} = \frac{\overline{\dot{\varepsilon}^2}}{\bar{\dot{\varepsilon}}} = f \tag{24}$$

That is, the mean-square strain rate divided by the mean strain rate should track the desired strain rate.

The macroscopic aspects of the forging are modeled using the commercial forming software, *Antares* (UES, 1993). *Antares* uses a standard nonlinear implicit iterative finite element based computational strategy. The workpiece material is modeled as rigid-viscoplastic and a shear friction constitutive law is used for characterization of die-workpiece interface behavior. The optimization technique described in this paper has been implemented without any modifications to the process model. All interaction with *Antares* is through the standard input and output files. This eliminates the need to maintain customized software, so that improvements in the process model are instantly reflected in the design software. A good example of this is the recent extension of *Antares* to 3-D problems, including automatic remeshing. The external optimization loop remains virtually unchanged, but by simply replacing the 2-D process model with a 3-D process model, a wide variety of new problems become accessible to the technique. This "black box" approach to the process model has some drawbacks. For example, it might be desired to use Newton's method to solve (21b) or (22b). However, this would require knowledge of the time derivative of the effective strain rate, which is not available as a standard *Antares* output. So the choice of root finding techniques is restricted to less efficient derivative-free methods.

The root finding algorithm implemented begins by bracketing a zero. Once bracketed, it switches to a general purpose routine called the Van Wijngaarden-Dekker-Brent (VDB) method (Press, *et al.*, 1986, pp. 251-254). The VDB method switches between parabolic interpolation and bisection, depending on whether the parabolic fit is good. When the interval is within an acceptable tolerance the routine terminates. Figure 3 shows how the VDB method is integrated with *Antares*.

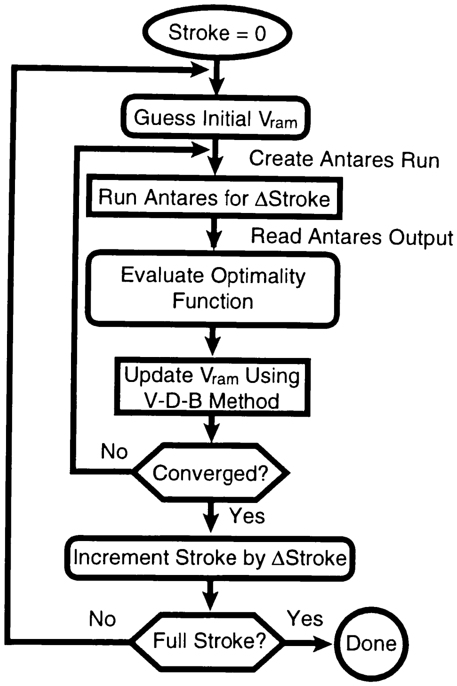

Fig. 3. General scheme for optimizing ram velocity via the VDB method.

It is natural to ask whether it would be better to search directly for minimizers of (2). The approach presented here has a major advantage in numerical robustness. Without excessively tight convergence criteria, and additional mesh management, the FEM solutions exhibit numerical noise. The result is false local minima of *J*. These will confuse a numerical minimization routine. However, they do not affect the zero crossings of (21) and (22), except in a small neighborhood of the solution. Furthermore, direct search techniques require a good initial guess for reliability and computational efficiency, and this approach does not.

5 Example—A γ-TiAl Compressor Disk Forging

TiAl intermetallics and alloys offer impressive potential weight savings and performance improvements in aircraft turbine and compressor components and automotive exhaust valves and turbocharger rotors. However, fabricating acceptable parts and realizing these improvements requires much greater attention to microstructure than in more conventional materials. In particular, large lamellar colonies typical of cast+HIPed TiAl ingots should be broken down into fine, equiaxed grains. This process, called spheroidization, is best accomplished through a bulk deformation process, such as extrusion or forging. However, because of the low ductility of these materials, they must be worked with extreme care. The optimal trajectory followed by a material element would maximize the fraction of material spheroidized, minimize the size of the resulting grains, and avoid regions associated with flow localization, cracking, or other undesirable behavior.

6.1 Weighting

The microstructural evolution equation for S, the fraction spheroidized, derived by Guillard (1994), (also, Rack, 1994), for the TiAl compound considered here (Ti-48Al-2V) is as follows:

$$S(\varepsilon,\dot{\varepsilon},T) = 2061.38 + 7.017\log\dot{\varepsilon} - 3.7908T + 56.84\varepsilon + 0.001776\,T^2 - 12.52\varepsilon^2 \quad (25)$$

where T is the temperature specified in degrees Celsius, log is base 10, and time is in seconds. It is understood that when the strain exceeds 2.27, the fraction transformed is one. The model is based on a curve fit to experimental data. That fit is strictly valid only in the region,

$$0.35 \leq \varepsilon \leq 2.03$$

$$10^{-4}\ \mathrm{s}^{-1} \leq \dot{\varepsilon} \leq 10^{-1}\ \mathrm{s}^{-1}$$

$$1058\ \mathrm{C} \leq T \leq 1142\ \mathrm{C}$$

Proceeding as in Section 3,

$$\frac{\partial S}{\partial \varepsilon}\frac{\dot{\varepsilon}}{\nu} = (56.84 - 25.04\ \varepsilon)\frac{\dot{\varepsilon}}{\nu} \tag{26}$$

and,

$$W(\varepsilon,\dot{\varepsilon},\nu) = \max\left((56.84 - 25.04\ \varepsilon)\frac{\dot{\varepsilon}}{\nu}\ ,\ W_{\min}\right) \tag{27}$$

where $W_{\min} > 0$ is necessary to satisfy the requirements of Section 2. This model presents several difficulties. The region of validity excludes the low end of the strain scale. Most forgings start with the billet material at close to zero strain. Furthermore, W is at a maximum when the strain is zero, so these regions are simultaneously poorly modeled, and extremely important. The second difficulty is that, contrary to prior assumption, and the behavior of the similar material discussed by Malas and Seetheraman (1992), the strain rate contribution is quite large. The probable cause of this is that the spheroidization mechanism has dynamic and static contributions. The dynamic part follows the form of (16b), but the static part is a non-decreasing function of time. The strain rates used in forming are low enough that the static mechanism can cause significant spheroidization during the forging. Trying to fit the time-dependent static mechanism to a time-invariant model leads erroneously to the large strain rate contributions. A better approach is including time in the model explicitly, and splitting the static and dynamic contributions. Then the forging could be designed to optimize the dynamic part, and a post-forming heat treatment designed to optimize the static transformation. Unfortunately material modeling is a difficult and expensive task, and the current model must suffice. Neglecting the strain rate term essentially ignores the static transformation.

6.2 The Optimal Material Trajectory

The forging has two critical aspects. The first is shaping the billet. Attaining the desired shape is a strict constraint, which is considered to have been exactly achieved when the ram reaches full stroke. This is accomplished by proper die and preform design. The second is attaining a desirable microstructure. Guillard (1994) has given desirable process parameters for isothermal, constant strain rate, compression. The processing target can be further refined, following a method given in Malas, Irwin, and Grandhi (1993). The result, calculated by Frazier (Mullins, *et al.*, 1995), is a constant strain rate of 0.3 1/min, at a temperature of 1100 C. Clearly this trajectory satisfies the assumptions of Section 2.

Six ram velocity profiles were applied to this forging. The algorithm described in the preceding section was used to obtain profile 1, a solution of (21b) based on $f(\varepsilon) = 0.3$ 1/min, with the weighting (27) and profile 2, a solution of (22b) with the same optimal material trajectory and weighting. Profile 1 will be referred to as time-based optimal, and profile 2 as stroke-based optimal. Profile 3 results from setting the unweighted average strain rate to the optimal material trajectory, that is, from maintaining an average strain rate over the billet of 0.3 1/min. Profiles 4 and 5 result from "rules of thumb" commonly used to pick ram velocities. They are based on solutions to an axisymmetric, frictionless, upsetting. If the dies where absolutely flat and frictionless, the target strain rate could be achieved exactly everywhere in the billet, throughout the forging. Profile 4 is this linear solution. Profile 5 is the constant velocity that would provide the correct strain rate at zero stroke. Finally, profile 6 is obtained by holding the ram force constant. Since there are no guidelines for picking the value, 300 tons was used. This is the ram force corresponding to the time-based optimal solution during the middle portion of the stroke.

6.3 Results

Figure 4 shows the resulting ram velocity profiles. The solutions vary significantly, especially at the beginning and end of the forging. It is interesting to relate features in the ram velocity profiles to events in the forging. Figure 5 shows the die-workpiece geometry at various strokes. Symmetry has been used to reduce the simulation time, and each picture represents one quarter of a cross-section through the billet.

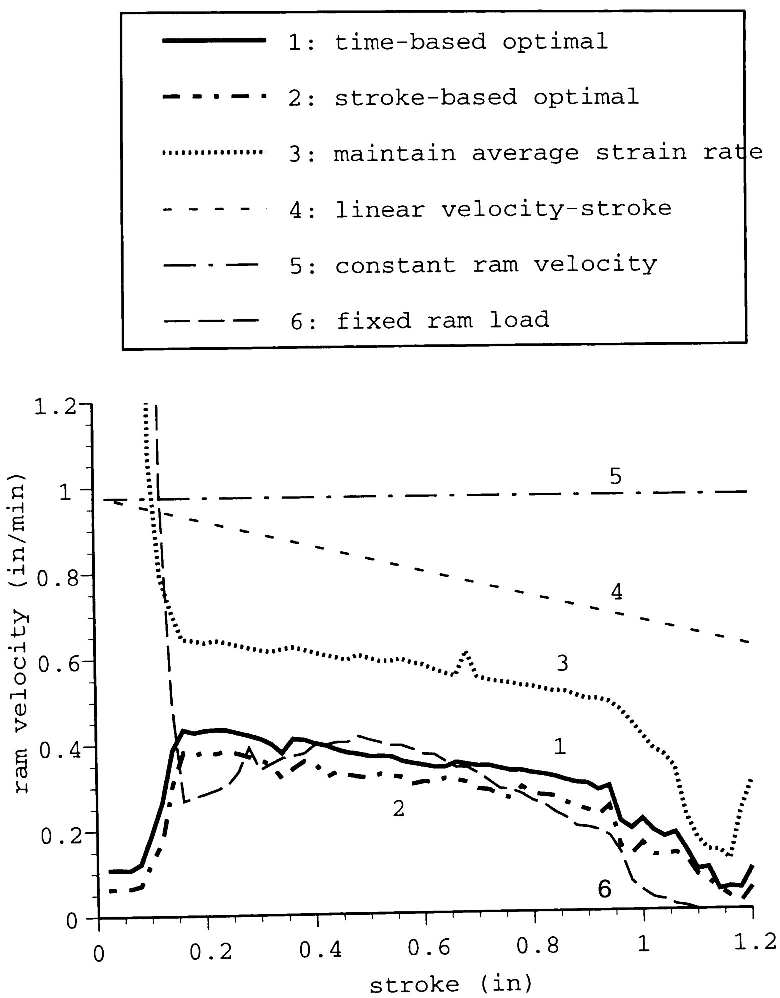

Fig. 4. Ram velocity profiles. Profiles 3 and 6 are clipped—Profile 3 goes as high as 6 in/min early in the stroke, Profile 6 hit the maximum ram velocity of 10 in/min. Profile 6 also fails to reach full stroke. The letters A-F correspond to the configurations shown in Fig. 5.

The constant ram load solution is unable to advance the ram at the end of the forging, and so does not reach full stroke. For the rest of this section the constant ram load solution is disregarded, since it fails to be admissible. The time-based and stroke-based optimal solutions are extremely close, with the time-based cost function giving a slightly shorter forging time, as expected. The stroke-based optimal solution will not be discussed individually, since it is practically identical to the time-based optimum.

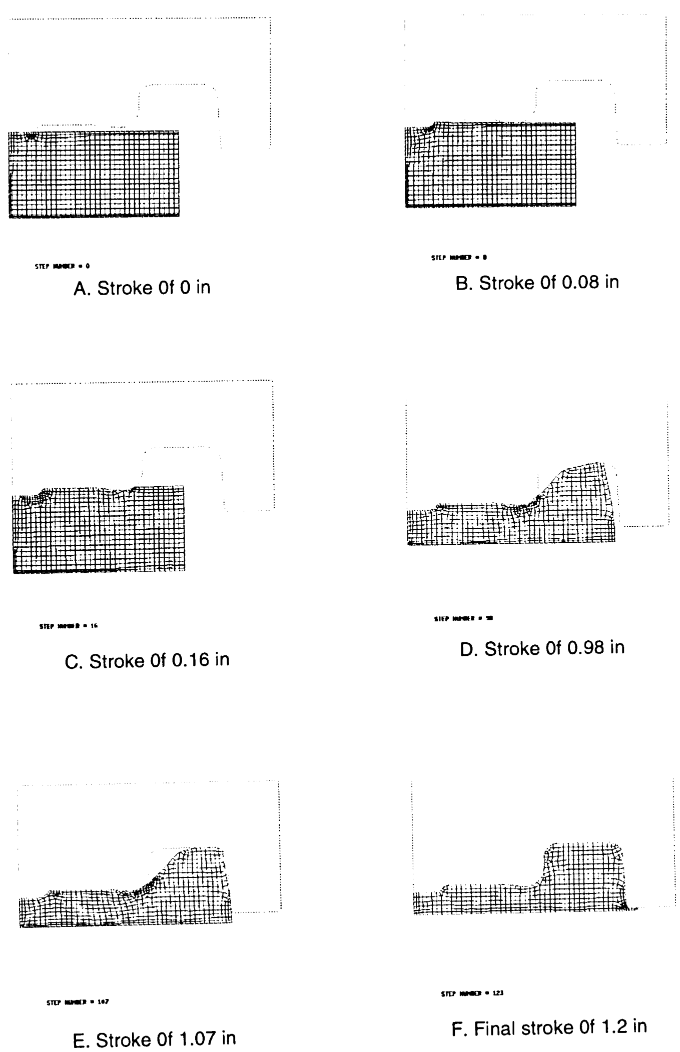

Fig. 5. Forging geometry.

The magnitude of the function g is a measure of how well the material is tracking the optimal trajectory at any stroke. Figure 6 plots the square root of g versus x for the four ram velocity profiles. Not surprisingly, the optimal solution is the best, with the others giving significantly higher values. Another measure is how closely the average strain rate, weighted as in (27) to emphasize the transforming material, follows the desired trajectory. Figure 7 shows these results. The optimal solution significantly out-performs the others, by a factor of two or more in the middle portion of the forging, and by an order of magnitude or more at the beginning and end of the forging. Note that Fig. 6 and 7 are both plotted on a log scale.

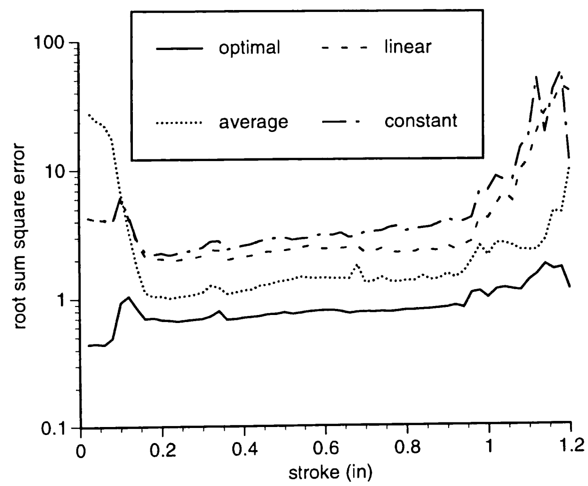

Fig.6. Square root of g versus stroke for the four ram velocity profiles.

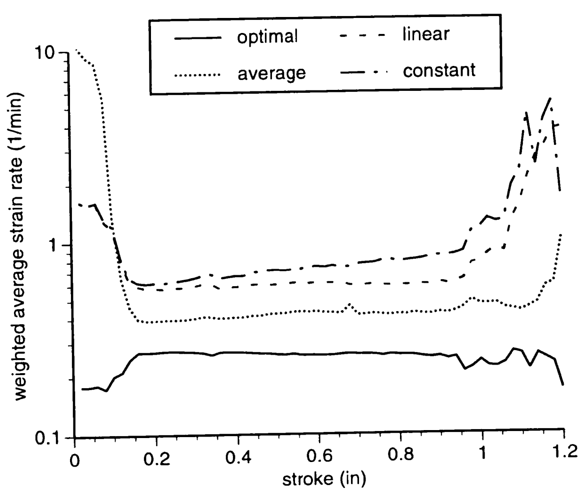

Fig.7. Weighted average strain rate versus stroke for the four ram velocity profiles.

The preceding results show that the optimal solution does a significantly better job of tracking the desired strain rate than the other approaches presented. However, it remains to be shown that the quality of the final part is significantly improved. Because the optimization of the material trajectory has been decoupled from the optimization of the bulk processing parameters, no sensitivity information has been carried over to the second step.

Detailed discussions of desired microstructural characteristics may be found in Malas and Seetheraman (1992), Malas, Irwin, and Grandhi (1993), and Berg, Adams, Malas, and Banda (1995). Two factors will be used here to evaluate and compare the preceding results. The first is the size of the spheroidized grains. The optimal trajectory derived in Mullins, *et al.* (1995) included a target grain size. The expression for grain size derived by Rack (1995) based on data taken by Guillard (1994) and used by Mullins, *et al.*, is,

$$d(\varepsilon,\dot{\varepsilon},T) = 248.2 + 143.0 \log\dot{\varepsilon} - 0.1284\, T - 59.82\, \varepsilon + 7.0\, \varepsilon^2 + 8.770 \log^2\dot{\varepsilon} - 0.0833\, T \log\dot{\varepsilon} - 143.0\, \varepsilon \log\dot{\varepsilon} \tag{28}$$

Using this equation at the forging temperature of 1100 C, the target strain rate of 0.005 1/sec, and zero strain, and assuming a linear relation between strain rate and ram velocity, gives a sensitivity relation ($\delta d/d$) = 0.3 ($\delta v/v$). Then a factor of two error in ram velocity corresponds to approximately a 30% error in grain size, which is fairly minor, and a factor of ten error in ram velocity corresponds to about a 270% grain size error, which is significant. Based on grain size only, the linear ram velocity profile probably gives an acceptable result.

The second factor that will be considered is material stability. Material stability is discussed extensively by Malas and Seetheraman (1992). Figure 8 shows a material stability map for the Ti-48Al-2V intermetallic used here. The black area represents "unstable" regions, that is undesirable transformation mechanisms that will result in an unacceptable forging. The optimal material trajectory will intersect this map at a point with temperature 1100 C and strain rate 0.3. This point is indicated in Fig. 8 by a black dot. The acceptable processing window is shaded light gray. From the diagram it can be seen that this point is close to instability, and so the strain rate must be tightly controlled. In fact, a doubling of the strain rate (and therefore, by assumption, a doubling of the ram velocity) will put the material into an unstable region. By this criterion, then, only the two optimal solutions are acceptable for the compressor disk forging.

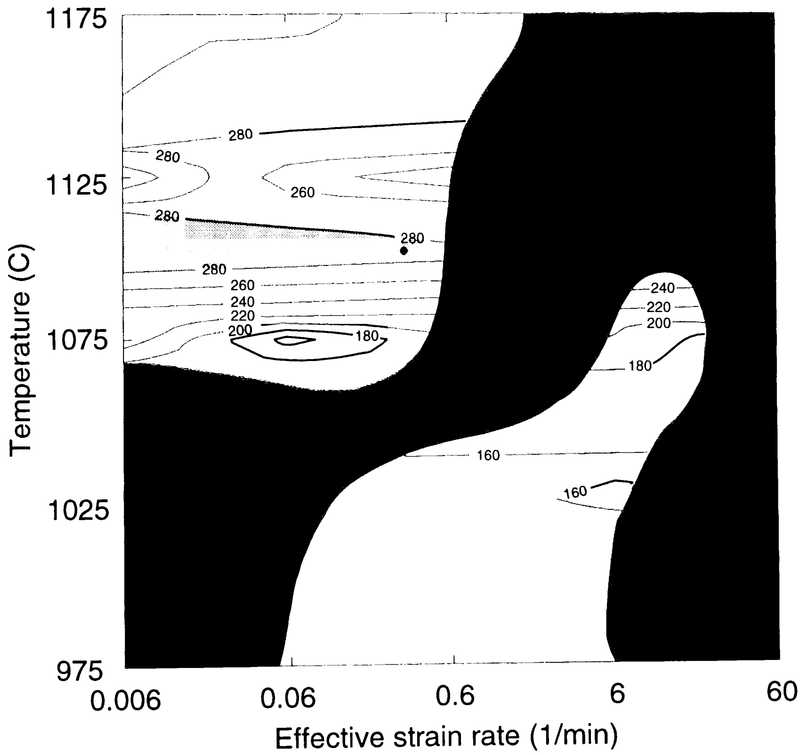

Fig. 8. Processing map for Ti-48Al-2V at strain of 0.7, from Guillard (1994).

6.4 Strain and Strain Rate Distribution

Figure 9 shows the effective strain distribution at the end of the forging for each profile. The purpose is to examine the validity of the rate invariance assumption. The results are extremely similar, despite the differences in the ram velocity histories. This strongly supports the assumption of rate invariance.

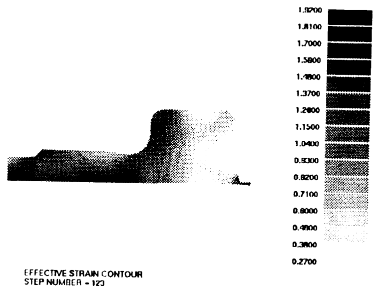

(a) Profile 1: Time-based optimal

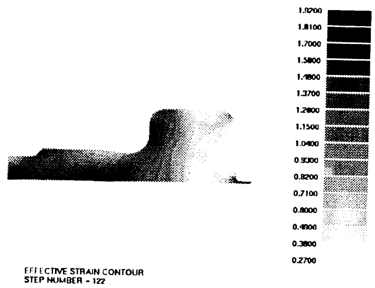

(b) Profile 3: Maintain average strain rate

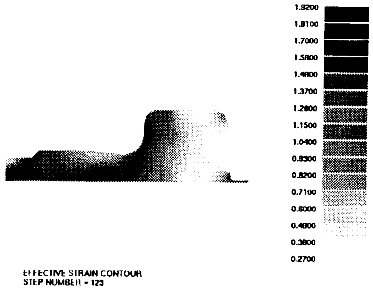

(c) Profile 4: Linear ram velocity

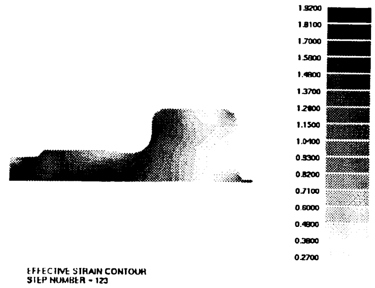

(d) Profile 5: Constant ram velocity

Fig. 9. Final strain distributions.

Figure 10 shows the effective strain rate distribution in the billet at a typical point in the forging. Note that the distributions have extremely similar variations, though the mean values reflect the differences in ram velocity. This is expected from (6a). Also note the complexity of the distribution. Using this information manually to balance the various regions of the billet, and select a ram velocity, would be extremely difficult.

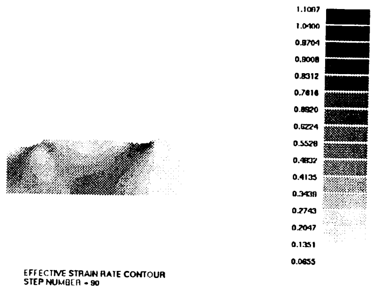

(a) Profile 1: Time-based optimal

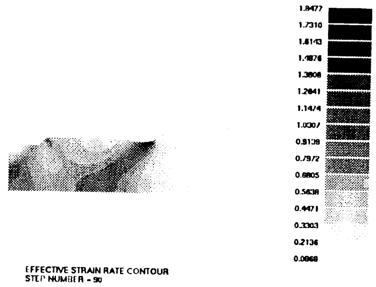

(b) Profile 3: Maintain average strain rate

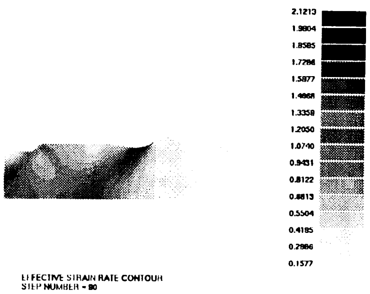

(c) Profile 4: Linear ram velocity

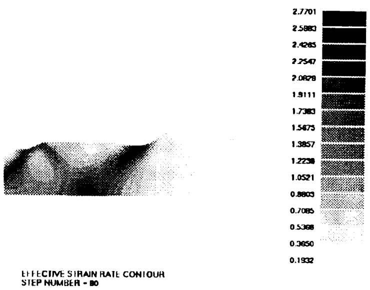

(d) Profile 5: Constant ram velocity

Fig. 10. Strain rate distibutions at stroke of 0.9 in.

6.5 Computational Cost and Accuracy

Figure 11 shows the number of function evaluations required for convergence at each stroke for the three iterative results—profiles 1, 2, and 3. Since each function evaluation requires a call to *Antares*, and requires significant computation, the total number should be kept low. Figure 11 shows that any of these needs about four times the computational effort of analyzing a given ram velocity. This should not be an excessive burden, except for the most involved geometries. The computations required for the time-based and stroke-based optimal solutions did not differ significantly.

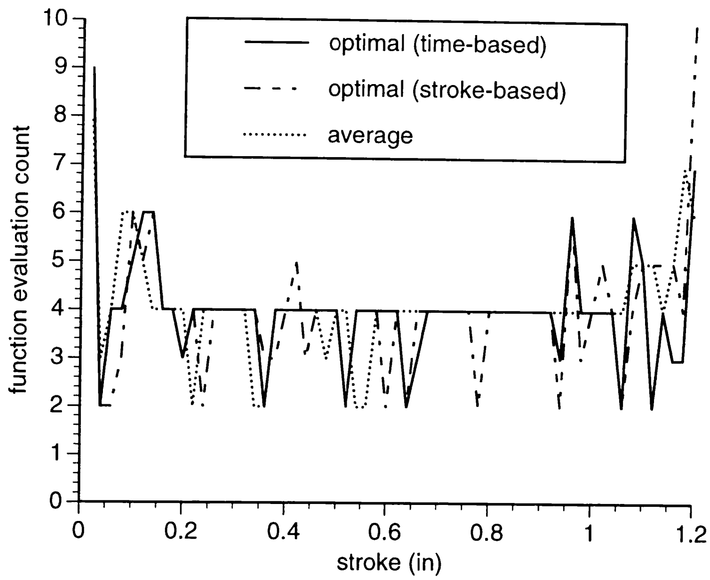

Fig.11. Function evaluation count for the three iterative ram velocity profiles.

6 Conclusions

A variational approach to the design of ram velocity profiles for isothermal forging was described. Knowledge of the microstructural evolution equations was integrated into the method in two ways. The first is through an optimal material trajectory, which is to be enforced throughout the deforming billet. The second is through a weighting function, selected to emphasize those portions of the billet undergoing the most microstructural transformation. A numerically robust and efficient algorithm was derived, based in part on assumptions about the behavior of isothermal forgings. Under certain reasonable restrictions and assumptions it can be shown that this algorithm produces a global optimum.

This technique has been applied to the simulated forging of a Titanium Aluminide compressor disk, in which microstructure plays an important role in both the mechanical properties of the finished part, and formability during hot working. The optimal ram velocity profiles tracked the desired strain rate. Competing methods differed by at least a factor of two, and by as much as two orders of magnitude. For materials such as this one, in which thermomechanical processing must take place in an extremely narrow range, such errors are unacceptable. Therefore, the techniques presented in this paper can make a crucial difference in successfully forging these materials.

Acknowledgements

This work described in this paper was supported by the National Research Council, the Air Force Office of Scientific Research, the USAF Wright Laboratory Flight Dynamics Directorate, and the USAF Wright Laboratory Materials Directorate. The authors would like to specially thank Dr. James Malas of the Process Design Group. Thanks also to Prof. George Avalos for advice and direction.

References

Axelsson, O., and V.A. Barker, (1984). *Finite Element Solution of Boundary Value Problems*, Academic Press, New York.

Berg, J., R.J. Adams, J.C. Malas, and S.S. Banda, (1995). "Nonlinear Optimization-Based Design of Ram Velocity Profiles for Isothermal Forging," *IEEE Transactions on Control Technology*, pp. 269-278.

Berg, J., A. Chaudhary, and J. Malas, (1995). "Open-Loop Control of a Hot Forming Process," in *Simulation of Materials Processing: Theory, Methods, and Applications: Proceedings of NUMIFORM '95*, S-F Shen and P.R. Dawson, editors, pp. 539–544, A.A. Balkema, Rotterdam.

Grandhi, R., A. Kumar, A. Chaudhary, and J. Malas, (1993). "State-Space Representation and Optimal Control of Non-Linear Material Deformation Using the Finite Element Method," *International Journal for Numerical Methods in Engineering*, Vol. 36, pp. 1967–1986.

Guillard, S., (1994). High Temperature Micro-Morphological Stability of the $(\alpha_2 + \gamma)$ Lamellar Structure in Titanium Aluminides, Ph.D. Thesis, Materials Science and Engineering Dept., Clemson University.

Hill, R., (1950). *Mathematical Theory of Plasticity*, Oxford University Press, London.

Malas, J.C. and V. Seetharaman, (1992). "Using Material Behavior Models to Develop Process Control Strategies," *JOM*, Vol. 44, No. 6, pp. 8–13.

Malas, J.C. R.D. Irwin, and R.V. Grandhi, (1993). "An Innovative Strategy for Open Loop Control of Hot Deformation Process," *Journal of Materials Engineering and Performance*, Vol. 2, No. 5, pp. 703–714.

Maniatty, A., and M-F Chen, (1995). "Shape Sensitivity Analysis for Steady Metal Forming Processes," in *Simulation of Materials Processing: Theory, Methods, and Applications: Proceedings of NUMIFORM '95*, S-F Shen and P.R. Dawson, editors, A.A. Balkema, Rotterdam.

Meyer, D.G., and H.N.G. Wadley, (1993). "Model-Based Feedback Control of Deformation Processing with Microstructure Goals," *Metallurgical Transactions B*, Vol. 24B, pp. 289–300.

Mullins, W.M., S.C. Medeiros, W.G. Frazier, B.M. DuBrosky, (1995). *Self-Improving Methods for Materials and Process Design: Sub-Scale IBR Forging from a γ-TiAl Alloy*, WL/MLIM Report, preprint.

Oh, S.I., (1982). "Finite Element Analysis of Metal forming Processes with Arbitrarily Shaped Dies," *Int. J. Mech. Sci.*, Vol. 24, No. 8, pp. 479-493.

Press, W.H., B.P. Flannery, S.A. Teukolsky, W.T. Vetterling, (1986). *Numerical Recipes: The Art of Scientific Computing*, Cambridge University Press, Cambridge.

Rack, H., (1984). Personal Communication.

Schwartz, C.A., J. Berg, M. Mears, and R. Chang, (1995). "Neural Network Identification and Control in Metal Forging," *Proceedings of the American Control Conference*, Seattle, WA, pp. 1782-1786.

Senuma, T., and H. Yada, (1986). "Microstructural Evolution of Plain Carbon Steels in Multiple Hot Working," in *Annealing Processes—Recovery, Recrystallization, and Grain Growth, Proc. 7th Risø Int. Symp. on Metallurgy and Materials Sci.*, S.S. Hansen, *et al.*, Eds., Risø National Laboratory, Roshilde, Denmark, pp. 547-552.

Smith, L. and J. Berg, (1996). "Shape and Velocity Optimization for Hot Metal Forming," to be presented at the 13th IFAC World Congress, San Francisco, CA.

UES, Inc., (1993). *Antares User's Manual Version 4.0*, UES, Inc., Dayton OH.

Recent IMA Preprints

#	Author/s	Title

1302 **J. Zhang**, A nonlinear nonlocal multi-dimensional conservation law
1303 **M.E. Taylor**, Estimates for approximate solutions to acoustic inverse scattering problems
1304 **J. Kim & D. Sheen**, A priori estimates for elliptic boundary value problems with nonlinear boundary conditions
1305 **B. Engquist & E. Luo**, New coarse grid operators for highly oscillatory coefficient elliptic problems
1306 **A. Boutet de Monvel & I. Egorova**, On the almost periodicity of solutions of the nonlinear Schrödinger equation with the cantor type spectrum
1307 **A. Boutet de Monvel & V. Georgescu**, Boundary values of the resolvent of a self-adjoint operator: Higher order estimates
1308 **S.K. Patch**, Diffuse tomography modulo Graßmann and Laplace
1309 **A. Friedman & J.J.L. Velázquez**, Liouville type theorems for fourth order elliptic equationsin a half plane
1310 **T. Aktosun, M. Klaus & C. van der Mee**, Recovery of discontinuities in a nonhomogeneous medium
1311 **V. Bondarevsky**, On the global regularity problem for 3-dimensional Navier-Stokes equations
1312 **M. Cheney & D. Isaacson**, Inverse problems for a perturbed dissipative half-space
1313 **B. Cockburn, D.A. Jones & E.S. Titi**, Determining degrees of freedom for nonlinear dissipative equations
1314 **B. Engquist & E. Luo**, Convergence of a multigrid method for elliptic equations with highly oscillatory coefficients
1315 **L. Pastur & M. Shcherbina**, Universality of the local eigenvalue statistics for a class of unitary invariant random matrix ensembles
1316 **V. Jakšić, S. Molchanov & L. Pastur**, On the propagation properties of surface waves
1317 **J. Nečas, M. Ružička & V. Šverák**, On self-similar solutions of the Navier-Stokes equations
1318 **S. Stojanovic**, Remarks on $W^{2,p}$-solutions of bilateral obstacle problems
1319 **E. Luo & H-O. Kreiss**, Pseudospectral vs. Finite difference methods for initial value problems with discontinuous coefficients
1320 **V.E. Grikurov**, Soliton's rebuilding in one-dimensional Schrödinger model with polynomial nonlinearity
1321 **J.M. Harrison & R.J. Williams**, A multiclass closed queueing network with unconventional heavy traffic behavior
1322 **M.E. Taylor**, Microlocal analysis on Morrey spaces
1323 **C. Huang**, Homogenization of biharmonic equations in domains perforated with tiny holes
1324 **C. Liu**, An inverse obstacle problem: A uniqueness theorem for spheres
1325 **M. Luskin**, Approximation of a laminated microstructure for a rotationally invariant, double well energy density
1326 **Rakesh & P. Sacks**, Impedance inversion from transmission data for the wave equation
1327 **O. Lafitte**, Diffraction for a Neumann boundary condition
1328 **E. Sobel, K. Lange, J.R. O'Connell & D.E. Weeks**, Haplotyping algorithms
1329 **B. Cockburn, D.A. Jones & E.S. Titi**, Estimating the number of asymptotic degrees of freedom for nonlinear dissipative systems
1330 **T. Aktosun**, Inverse Schrödinger scattering on the line with partial knowledge of the potential
1331 **T. Aktosun & C. van der Mee**, Partition of the potential of the one-dimensional Schrödinger equation
1332 **B. Engquist & E. Luo**, Convergence of the multigrid method with a wavelet coarse grid operator
1333 **V. Jakšić & C.-A. Pillet**, Ergodic properties of the Spin-Boson system
1334 **S.K. Patch**, Recursive solution for diffuse tomographic systems of arbitrary size
1335 **J.C. Bronski**, Semiclassical eigenvalue distribution of the non self-adjoint Zakharov-Shabat eigenvalue problem
1336 **J.C. Cockburn**, Bitangential structured interpolation theory
1337 **S. Kichenassamy**, The blow-up problem for exponential nonlinearities
1338 **F.A. Grünbaum & S.K. Patch**, How many parameters can one solve for in diffuse tomography?
1339 **R. Lipton**, Reciprocal relations, bounds and size effects for composites with highly conducting interface
1340 **H.A. Levine & J. Serrin**, A global nonexistence theorem for quasilinear evolution equations with dissipation
1341 **A. Boutet de Monvel & R. Purice**, The conjugate operator method: Application to DIRAC operators and to stratified media
1342 **G. Michele Graf**, Stability of matter through an electrostatic inequality
1343 **G. Avalos**, Sharp regularity estimates for solutions of the wave equation and their traces with prescribed Neumann data
1344 **G. Avalos**, The exponential stability of a coupled hyperbolic/parabolic system arising in structural acoustics
1345 **G. Avalos & I. Lasiecka**, A differential Riccati equation for the active control of a problem in structural acoustics
1346 **G. Avalos**, Well-posedness for a coupled hyperbolic/parabolic system seen in structural acoustics
1347 **G. Avalos & I. Lasiecka**, The strong stability of a semigroup arising from a coupled hyperbolic/parabolic system
1348 **A.V. Fursikov**, Certain optimal control problems for Navier-Stokes system with distributed control function
1349 **F. Gesztesy, R. Nowell & W. Pötz**, One-dimensional scattering theory for quantum systems with nontrivial spatial asymptotics
1350 **F. Gesztesy & H. Holden**, On trace formulas for Schrödinger-type operators

1351 **X. Chen**, Global asymptotic limit of solutions of the Cahn-Hilliard equation
1352 **X. Chen**, Lorenz equations, Part I: Existence and nonexistence of homoclinic orbits
1353 **X. Chen**, Lorenz equations Part II: "Randomly" rotated homoclinic orbits and chaotic trajectories
1354 **X. Chen**, Lorenz equations, Part III: Existence of hyperbolic sets
1355 **R. Abeyaratne, C. Chu & R.D. James**, Kinetics of materials with wiggly energies: Theory and application to the evolution of twinning microstructures in a Cu-Al-Ni shape memory alloy
1356 **C. Liu**, The Helmholtz equation on Lipschitz domains
1357 **G. Avalos & I. Lasiecka**, Exponential stability of a thermoelastic system without mechanical dissipation
1358 **R. Lipton**, Heat conduction in fine scale mixtures with interfacial contact resistance
1359 **V. Odisharia & J. Peradze**, Solvability of a nonlinear problem of Kirchhoff shell
1360 **P.J. Olver, G. Sapiro & A. Tannenbaum**, Affine invariant edge maps and active contours
1361 **R.D. James**, Hysteresis in phase transformations
1362 **A. Sei & W. Symes**, A note on consistency and adjointness for numerical schemes
1363 **A. Friedman & B. Hu**, Head-media interaction in magnetic recording
1364 **A. Friedman & J.J.L. Velázquez**, Time-dependent coating flows in a strip, part I: The linearized problem
1365 **X. Ren & M. Winter**, Young measures in a nonlocal phase transition problem
1366 **K. Bhattacharya & R.V. Kohn**, Elastic energy minimization and the recoverable strains of polycrystalline shape-memory materials
1367 **G.A. Chechkin**, Operator pencil and homogenization in the problem of vibration of fluid in a vessel with a fine net on the surface
1368 **M. Carme Calderer & B. Mukherjee**, On Poiseuille flow of liquid crystals
1369 **M.A. Pinsky & M.E. Taylor**, Pointwise Fourier inversion: A wave equation approach
1370 **D. Brandon & R.C. Rogers**, Order parameter models of elastic bars and precursor oscillations
1371 **H.A. Levine & B.D. Sleeman**, A system of reaction diffusion equations arising in the theory of reinforced random walks
1372 **B. Cockburn & P.-A. Gremaud**, A priori error estimates for numerical methods for scalar conservation laws. Part II: Flux-splitting monotone schemes on irregular Cartesian grids
1373 **B. Li & M. Luskin**, Finite element analysis of microstructure for the cubic to tetragonal transformation
1374 **M. Luskin**, On the computation of crystalline microstructure
1375 **J.P. Matos**, On gradient young measures supported on a point and a well
1376 **M. Nitsche**, Scaling properties of vortex ring formation at a circular tube opening
1377 **J.L. Bona & Y.A. Li**, Decay and analyticity of solitary waves
1378 **V. Isakov**, On uniqueness in a lateral cauchy problem with multiple characteristics
1379 **M.A. Kouritzin**, Averaging for fundamental solutions of parabolic equations
1380 **T. Aktosun, M. Klaus & C. van der Mee**, Integral equation methods for the inverse problem with discontinuous wavespeed
1381 **P. Morin & R.D. Spies**, Convergent spectral approximations for the thermomechanical processes in shape memory allows
1382 **D.N. Arnold & X. Liu**, Interior estimates for a low order finite element method for the Reissner-Mindlin plate model
1383 **D.N. Arnold & R.S. Falk**, Analysis of a linear-linear finite element for the Reissner-Mindlin plate model
1384 **D.N. Arnold, R.S. Falk & R. Winther**, Preconditioning in $H(\mathrm{div})$ and applications
1385 **M. Lavrentiev**, Nonlinear parabolic problems possessing solutions with unbounded gradients
1386 **O.P. Bruno & P. Laurence**, Existence of three-dimensional toroidal MHD equilibria with nonconstant pressure
1387 **O.P. Bruno, F. Reitich, & P.H. Leo**, The overall elastic energy of polycrystallin martensitic solids
1388 **M. Fila & H.A. Levine**, On critical exponents for a semilinear parabolic system coupled in an equation and a boundary condition
1389 **J.M. Berg, W.G. Frazier, A. Chaudhary, & S.S. Banda**, Optimal open-loop ram velocity profiles for isothermal forging: A variational approach
1390 **J.M. Berg & H.G. Kwatny**, Unfolding the zero structure of a linear control system
1391 **A. Sei**, High order finite-difference approximations of the wave equation with absorbing boundary conditions: A stability analysis
1392 **A.V. Coward & Y.Y. Renardy**, Small amplitude oscillatory forcing on two-layer plane channel flow
1393 **V.A. Pliss & G.R. Sell**, Approximation dynamics and the stability of invariant sets
1394 **J.G. Cao & P. Roblin**, A new computational model for heterojunction resonant tunneling diode
1395 **C. Liu**, Inverse obstacle problem: Local uniqueness for rougher obstacles and the identification of a ball
1396 **K.A. Pericak-Spector & S.J. Spector**, Dynamic cavitation with shocks in nonlinear elasticity
1397 **G. Avalos & I. Lasiecka**, Exponential stability of a thermoelastic system without mechanical dissipation II: The case of simply supported boundary conditions
1398 **B. Brighi & M. Chipot**, Approximation of infima in the calculus of variations